Development of a Compton Camera for Medical Applications based on Silicon Strip and Scintillation Detectors

J. Krimmer[a,*], J.-L. Ley[a], C. Abellan[b], J.-P. Cachemiche[b], L. Caponetto[a], X. Chen[a], M. Dahoumane[a], D. Dauvergne[a], N. Freud[c], B. Joly[d], D. Lambert[d], L. Lestand[d], J.M. Létang[c], M. Magne[d], H. Mathez[a], V. Maxim[c], G. Montarou[d], C. Morel[b], M. Pinto[a], C. Ray[a], V. Reithinger[a], E. Testa[a], Y. Zoccarato[a]

[a] *Institut de Physique Nucléaire de Lyon; Université de Lyon, F-69003 Villeurbanne, France; IN2P3/CNRS, UMR 5822; Université de Lyon 1, F-69622 Villeurbanne, France*
[b] *Aix-Marseille Université, CNRS/IN2P3, CPPM UMR 7346, 13288 Marseille*
[c] *Université de Lyon, CREATIS; CNRS UMR5220; Inserm U1044; INSA - Lyon; Université Lyon 1; Centre Léon Bérard, France*
[d] *Clermont Université, Université Blaise Pascal, CNRS/IN2P3, Laboratoire de Physique Corpusculaire, BP 10448, F-63000 Clermont-Ferrand, France*

Abstract

A Compton camera is being developed for the purpose of ion-range monitoring during hadrontherapy via the detection of prompt-gamma rays. The system consists of a scintillating fiber beam tagging hodoscope, a stack of double sided silicon strip detectors ($90\times90\times2$ mm^3, 2×64 strips) as scatter detectors, as well as bismuth germanate (BGO) scintillation detectors ($38\times35\times30$ mm^3, 100 blocks) as absorbers. The individual components will be described, together with the status of their characterization.

Keywords: Compton camera, silicon strip detectors, prompt gamma, hadrontherapy
PACS: 29.40.Mc, 87.53.Bn, 87.53.Kn, 87.56.Fc

*Corresponding author
Email address: j.krimmer@ipnl.in2p3.fr (J. Krimmer)

1. Introduction

Hadrontherapy, i.e. the treatment of tumors via a beam of light ions - mainly proton and carbon, is an emerging technology that takes advantage of the effect, that ions deposit a large fraction of their energy close to the end of their range, in the Bragg peak region, while travelling along almost straight trajectories. In comparison to conventional radiotherapy with X-rays, this property allows a better concentration of the applied dose to the tumor volume whereas surrounding healthy tissues are widely spared. Hence, tumors close to organs at risk, are for instance particularly indicated for this type of treatment.

A critical issue in the quality control of hadrontherapy is the surveillance of the Bragg peak location and its conformation to the tumor volume. A mismatch could lead to an under-dosage in the target volume and an over-dosage in healthy tissues.

Methods for monitoring the ion range are based on the detection of secondary radiation. One modality, which has already proven its clinical applicability, is the registration of the emission point of 511 keV annihilation radiation following a β^+-decay, by using positron emission tomography (PET) [1, 2, 3]. In the case of carbon ion treatment, tracking of emitted light charged fragments can be used for a reconstruction of the primary interaction vertex [4, 5, 6, 7]. Inelastic nuclear reactions of the incident ions lead also to the generation of prompt-gamma rays which are emitted almost instantaneously after the interaction. It has been shown that the production rates of the prompt-gammas (energies up to approximately 10 MeV) are highly correlated to the range of the primary ions [8, 9, 10, 11]. Camera systems for the detection of prompt-gamma rays, based on passive collimation, can either be of the knife-edge type [12, 13] or can include a parallel multi-slit collimator [14, 15, 16]. An alternative approach to passive collimation relies on the Compton camera concept, which has the potential advantage of an expected improved efficiency compared to passive collimation. In the field of nuclear medicine, Compton cameras can replace classical single photon emission computed tomography (SPECT) systems with passive collimation and open the door to new radiotracers with gamma energies on the order of 1 MeV.

Several groups worldwide are studying Compton cameras (see e.g. [17, 18, 19, 20, 21]). The present article is focused on the development of a time-of-flight Compton camera of clinical size.

2. Compton camera

2.1. Principle

The principle of the Compton camera is shown in Figure 1 [22]. Incident ions are passing a beam tagging hodoscope, which provides information about the transverse position and may also serve as a time reference for time-of-flight (TOF) measurements. Photons produced via nuclear interactions of

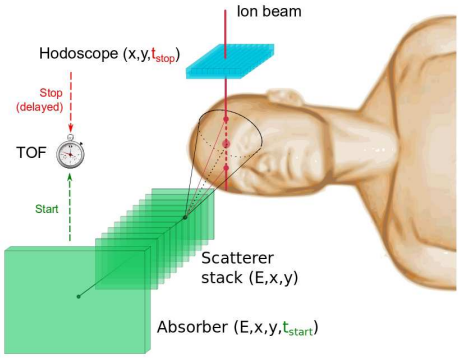

Figure 1: Principle of the Compton camera with its basic components: the beam tagging hodoscope, the scatter detectors and the absorber. The vertex of photon production is reconstructed via the intersection of the Compton cone with the line of incident ions.

the incident ions interact first in a stack of low-Z element scatterers before the scattered photons hit the high-Z element absorber. Using energy- and position-sensitive detectors, the Compton cone defined by the apex in the scatterer and the scattering angle is determined. The vertex of the photon creation is then given by the intersection of this cone with the incident ion trajectory. One of the two intersection points generally obtained can be considered as background.

2.2. Components

The basic components of the Compton camera comprising the hodoscope, the scatter detectors and the absorber are displayed in Figure 2.
The beam tagging hodoscope consists of an array of scintillating fibers (BCF 12, $1\times1\text{mm}^2$ square section)[1], which are coupled to multianode photomultipliers (PMs) (H-8500) via optical fibers[2]. Two prototypes have been built with 2×32 and 2×128 fibers, respectively. Test measurements have shown that a timing resolution better than 1 ns full width at half maximum (FWHM)

[1]http://www.crystals.saint-gobain.com/Scintillating_Fiber.aspx
[2]http://www.foretec.fr/fibre-optique.html

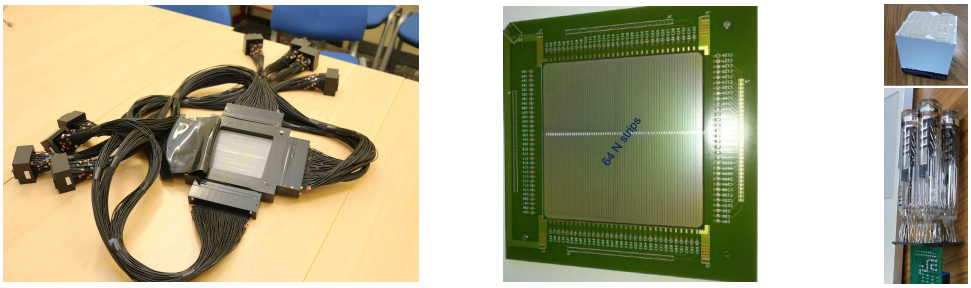

Figure 2: Individual components of the Compton camera with the hodoscope (left), a silicon strip detector (middle) and a BGO detector (right).

is possible and that count rates above 10 MHz can be reached. For the full size prototype, the scintillating fibers are read from both ends and the signals from neighboring fibers are connected to different PMs for an improved count rate capability. Dedicated front-end electronics is being developed. The first version of an application specific integrated circuit (ASIC) [23] contains a current comparator for each channel to provide digital information on the fibers that have been hit, as well as the possibility to measure the charge produced by single fibers by using a charge sensitive amplifier (CSA) in order to monitor aging of the fibers. The second version of the ASIC, which is currently under test, includes timing capabilities by using a 160 MHz clock in combination with a delay locked loop (DLL). The ASICs have been designed for count rates up to 10^8 Hz.

Double sided silicon strip detectors ($90\times90\times2$ mm^3, 2×64 strips) will be used as scatterers (see Fig. 2 for a detector mounted on a printed circuit board). Tests with a small-size prototype ($14\times14\times2$ mm^3, 2×8 strips) exhibit a leakage current below 1 nA per strip for temperatures below 0 °C and an energy resolution of 8 keV FWHM for the gamma lines of a ^{133}Ba source (81 and 356 keV). The corresponding front-end ASIC [24] comprises a fast (15 ns) and a slow shaper (1 µs) for the time and energy information, respectively. The second version of the ASIC, which is designed for low noise (120 electrons root mean square) and count rates of 10^5 Hz, is currently being characterized.

The absorber detector will be composed of 100 BGO blocks ($38\times35\times30$ mm^3 for each block). Simulation studies for a comparison of different absorber materials including $LaBr_3$:Ce with its excellent energy and time resolution, have

been performed. These simulations showed that cerium doped lutetium yttrium orthosilicate (LYSO:Ce) and BGO provide the best performance with respect to position resolution and efficiency [25]. This is due to a larger photoabsorption probability in comparison to $LaBr_3$:Ce or NaI(Tl). Furthermore, an absorber with dimensions 400×400×30 mm^3 made from $LaBr_3$:Ce would be cost-intensive. Moreover, as compared to LYSO:Ce, BGO avoids the inconvenience of intrinsic radioactivity, although LYSO:Ce, as well as $LaBr_3$ would be faster. The BGO crystals coming from an ancient PET system are streaked, providing 8×8 pseudo pixels. Each scintillator block is read out via four PMs (Figure 2 (right)) which allows a reconstruction of the impact position via a centroid calculation. Results from test measurements with prompt-gamma rays induced by 95 MeV/u ^{12}C-ions at the Grand Accélérateur National d'Ions Lourds (GANIL, Caen, France)[3] are given in Figure 3. For the measurement of the timing resolution (2 ns FWHM), the HF-signal of the accelerator has been used as reference. The beam time structure consists of 1 ns pulses every 80 ns. The reconstruction of the impact position via centroid calculation of the signals from the four PMs reveals the pixel structure of the scintillator blocks (Fig. 3 (down)).
The data flux of the clinical size prototype will be handled by a Micro Telecommunications Computing Architecture (μ-TCA) data acquisition system [26].

2.3. Simulations and clinical applicability

Geant4 [27] (version 9.6.p02) simulations have been performed for an optimization of the Compton camera arrangement. These simulations have also been used to explore the applicability of the present setup under clinical conditions. Typical parameters for a treatment with a proton beam are: intensities of $\sim 10^{10}$ protons/s with beam bunches of 2 ns every 10 ns. This results in ∼200 protons per bunch. In the simulations the timing resolutions of the BGO (3 ns) and silicon detectors (15 ns) have been applied. The reconstructed vertices of 10^8 incident protons, which corresponds to a typical distal spot in pencil beam scanning [13], are given in Figure 4. In the upper part of the figure, at clinical intensities, the distribution of *true gamma* events (i.e. good reconstructible Compton events) is dominated by *other* (random) coincidences. In the lower part of the figure the beam intensity has been

[3] http://www.ganil-spiral2.eu/leganil

reduced to one proton per bunch. Here, the fall-off after the Bragg peak (at position 0) is revealed.

3. Conclusion

The status of the development of a clinical-size Compton camera has been presented. The individual detector components and their corresponding front-end electronics are under characterization. Simulation studies have shown that for a usage of the Compton camera to monitor the ion range during hadrontherapy, the intensity needs to be reduced to one ion per bunch. In the case of a proton beam with pencil-beam scanning, the duration for a single spot increases to about 1 s, which can be tolerated for selected individual spots.

Acknowledgment

This research project has been partly supported by the Regional Program for Research in Hadrontherapy (PRRH, under CPER 2007-13 funding), the European FP 7 projects ENVISION (grant agreement nr. 241851), ENTER-VISION (grant agreement nr. 264552), ULICE (grant agreement nr. 228436) and the ANR Gamhadron project (ANR-09-BLAN-0106). This work was performed within the framework of the LABEX PRIMES (ANR-11-LABX-0063) and France Hadron (ANR-11-INBS-0007).

References

[1] G. Shakirin, H. Braess, F. Fiedler *et al.*, Phys. Med. Biol. 56 (5) (2011) 1281. doi:http://dx.doi.org/10.1088/0031-9155/56/5/004.

[2] W. Enghardt, P. Crespo, F. Fiedler *et al.*, Nucl. Instr. Meth. **A** 525 (1-2) (2004) 284 – 288. doi:http://dx.doi.org/10.1016/j.nima.2004.03.128.

[3] T. Nishio, T. Ogino, K. Nomura *et al.* Med. Phys. 33 (2006) 4190. doi:http://dx.doi.org/10.1118/1.2361079.

[4] U. Amaldi, W. Hajdas, S. Iliescu *et al.*, Nucl. Instr. Meth. **A** 617 (1-3) (2010) 248 – 249. doi:http://dx.doi.org/10.1016/j.nima.2009.06.087.

[5] P. Henriquet, E. Testa, M. Chevallier *et al.*, Phys. Med. Biol. 57 (14) (2012) 4655. doi:http://dx.doi.org/10.1088/0031-9155/57/14/4655.

[6] C. Agodi, G. Battistoni, F. Bellini *et al.*, Phys. Med. Biol. 57 (18) (2012) 5667. doi:http://dx.doi.org/10.1088/0031-9155/57/18/5667.

[7] K. Gwosch, B. Hartmann, J. Jakubek *et al.*, Phys. Med. Biol. 58 (11) (2013) 3755. doi:http://dx.doi.org/10.1088/0031-9155/58/11/3755.

[8] C.-H. Min, C.H. Kim and M.-Y. Youn *et al.*, Appl. Phys. Lett. 89 (18) (2006) 183517. doi:http://dx.doi.org/10.1063/1.2378561.

[9] C. H. Kim, C. H. Min, K. S. Seo *et al.*, Journal of the Korean Physical Society 50 (5) (2007) 1510–1513.

[10] E. Testa, M. Bajard, M. Chevallier *et al.*, Appl. Phys. Lett. 93 (9) (2008) 093506. doi:http://dx.doi.org/10.1063/1.2975841.

[11] J. Verburg, K. Riley, T. Bortfeld, *et al.*, Phys. Med. Biol. 58 (20) (2013) L37. doi:http://dx.doi.org/10.1088/0031-9155/58/20/L37.

[12] V. Bom, L. Joulaeizadeh, F. Beekman, Phys. Med. Biol. 57 (2) (2012) 297. doi:http://dx.doi.org/10.1088/0031-9155/57/2/297.

[13] J. Smeets, F. Roellinghoff, D. Prieels *et al.*, Phys. Med. Biol. 57 (11) (2012) 3371. doi:http://dx.doi.org/10.1088/0031-9155/57/11/3371.

[14] M. Testa, M. Bajard, M. Chevallier *et al.*, Rad. Env. Biophys. 49 (2010) 337–343. doi:http://dx.doi.org/10.1007/s00411-010-0276-2.

[15] C. H. Min, H. R. Lee, C. H. Kim *et al.*, Med. Phys. 39 (4) (2012) 2100–2107. doi:http://dx.doi.org/10.1118/1.3694098.

[16] J. Krimmer, M. Chevallier, J. Constanzo *et al.*, submitted to JINST.

[17] S. W. Peterson, D. Robertson, J. Polf, Phys. Med. Biol. 55 (22) (2010) 6841. doi:http://dx.doi.org/10.1088/0031-9155/55/22/015.

[18] H. Seo, J.H. Park, A. Ushakov *et al.*, JINST 6 (01) (2011) C01024. doi:http://dx.doi.org/10.1088/1748-0221/6/01/C01024.

[19] S. Kurosawa, H. Kubo, K. Ueno *et al.*, Curr. Appl. Phys. 12 (2) (2012) 364 – 368. doi:http://dx.doi.org/10.1016/j.cap.2011.07.027.

[20] T. Kormoll, F. Fiedler, S. Schöne *et al.*, Nucl. Instr. Meth. **A** 626-627 (0) (2011) 114 – 119. doi:http://dx.doi.org/10.1016/j.nima.2010.10.031.

[21] G. Llosá, J. Cabello, S. Callier *et al.*, Nucl. Instr. Meth. **A** 718 (0) (2013) 130 – 133. doi:http://dx.doi.org/10.1016/j.nima.2012.08.074.

[22] F. Roellinghoff, M.-H. Richard, M. Chevallier *et al.*, Nucl. Instr. Meth. **A** 648 (2011) S20 – S23. doi:http://dx.doi.org/10.1016/j.nima.2011.01.069.

[23] S. Deng, H. Mathez, D. Dauvergne *et al.*, Nucl. Instr. Meth. **A** 695 (2012) 390 – 393. doi:http://dx.doi.org/10.1016/ j.nima.2011.11.042.

[24] M. Dahoumane, D. Dauvergne, D. Delaunay *et al.*, IEEE NSS MIC (2012).

[25] M.-H. Richard, M. Chevallier, D. Dauvergne *et al.*, IEEE Trans. Nucl. Sci. 59 (5) (2012) 1850–1855. doi:http://dx.doi.org/10.1109/NSSMIC.2011.6152642.

[26] C. Abellan, J.-P. Cachemiche, F. Rethore *et al.*, ANIMMA (2013).

[27] S. Agostinelli, J. Allison, K. Amako *et al.*, Nucl. Instr. Meth. **A** 506 (2003) 250–303. http://www.sciencedirect.com/science/article/pii/S0168900203013688.

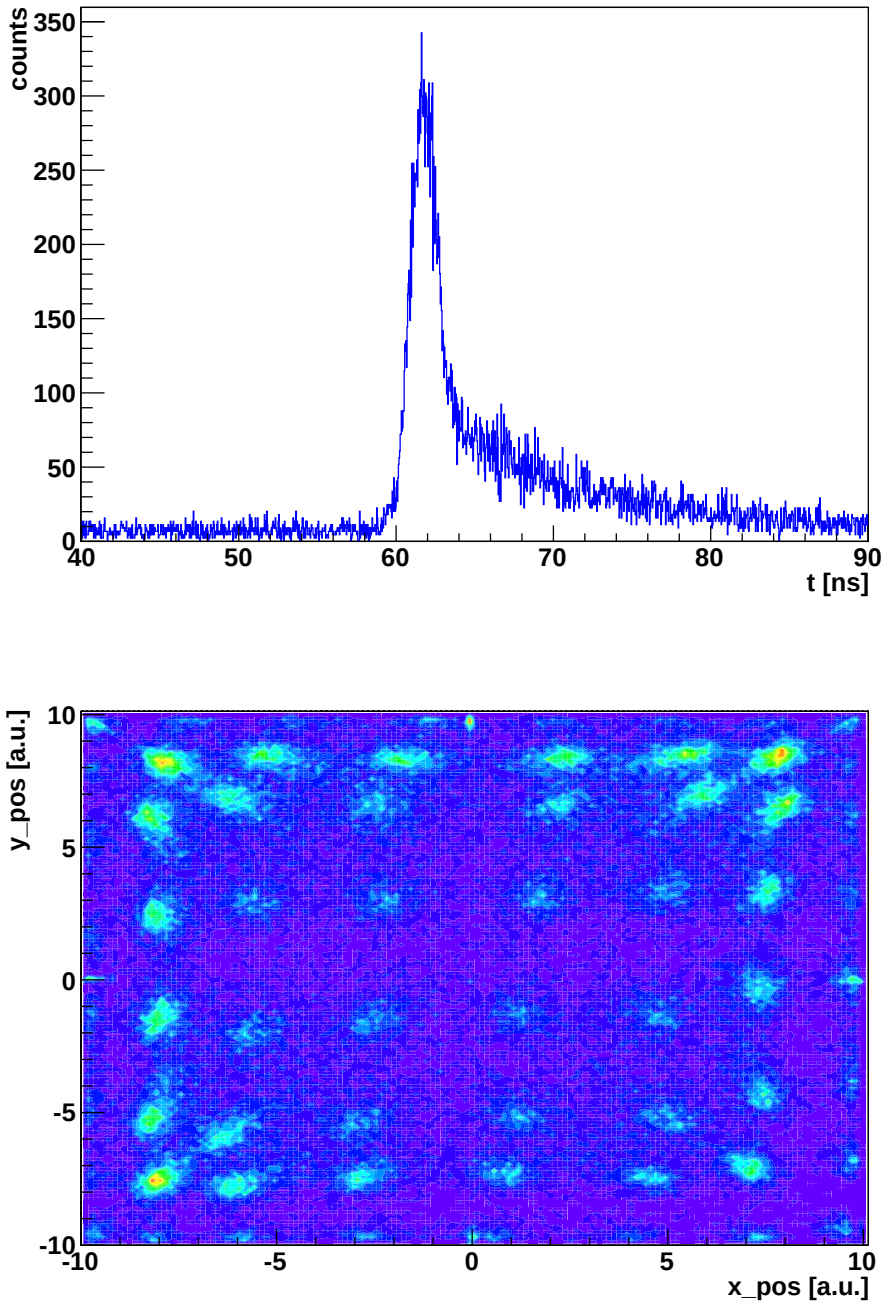

Figure 3: Results from tests with a BGO detector. Up: Measurement of the timing resolution, down: Reconstructed impact positions revealing the pixel structure of the scintillator blocks.

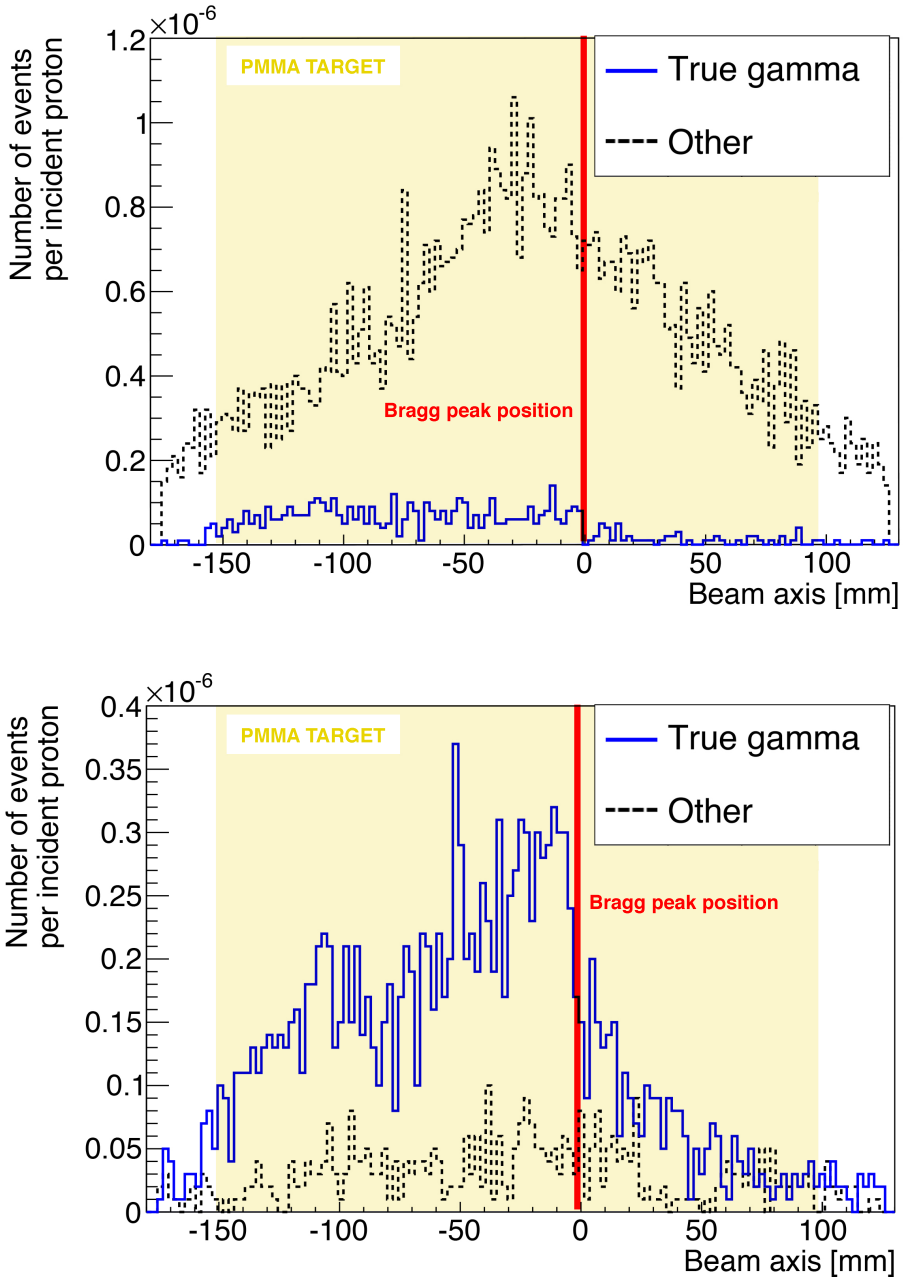

Figure 4: Reconstructed vertices of 10^8 incident protons (160 MeV) at clinical (up) and reduced (down) intensities with 200 and 1 protons per bunch, respectively. The location of the Bragg peak is indicated at position 0.